Transition of Proton Energy Scaling Using an Ultrathin Target Irradiated by Linearly Polarized Femtosecond Laser Pulses

I Jong Kim,[1,2] Ki Hong Pae,[1] Chul Min Kim,[1,2] Hyung Taek Kim,[1,2] Jae Hee Sung,[1,2] Seong Ku Lee,[1,2] Tae Jun Yu,[1,2] Il Woo Choi,[1,2] Chang-Lyoul Lee,[1] Kee Hwan Nam,[1] Peter V. Nickles,[3] Tae Moon Jeong,[1,2,*] and Jongmin Lee[1,†]

[1]*Advanced Photonics Research Institute, Gwangju Institute of Science and Technology, Gwangju 500-712, Korea*

[2]*Center for Relativistic Laser Science, Institute for Basic Science (IBS), Gwangju 500-712, Korea*

[3]*WCU, Department of Nanobio Materials and Electronics, Gwangju Institute of Science and Technology, Gwangju 500-712, Korea*

(Received 27 May 2013; published 16 October 2013)

Particle acceleration using ultraintense, ultrashort laser pulses is one of the most attractive topics in relativistic laser-plasma research. We report proton and/or ion acceleration in the intensity range of 5×10^{19} to 3.3×10^{20} W/cm^2 by irradiating linearly polarized, 30-fs laser pulses on 10-to 100-nm-thick polymer targets. The proton energy scaling with respect to the intensity and target thickness is examined, and a maximum proton energy of 45 MeV is obtained when a 10-nm-thick target is irradiated by a laser intensity of 3.3×10^{20} W/cm^2. The proton acceleration is explained by a hybrid acceleration mechanism including target normal sheath acceleration, radiation pressure acceleration, and Coulomb explosion assisted-free expansion. The transition of proton energy scaling from $I^{1/2}$ to I is observed as a consequence of the hybrid acceleration mechanism. The experimental results are supported by two- and three-dimensional particle-in-cell simulations.

DOI: 10.1103/PhysRevLett.111.165003 PACS numbers: 52.38.Kd, 41.75.Jv, 52.59.−f

Charged particle acceleration using ultraintense and ultrashort laser pulses is one of the most attractive topics in the relativistic laser-plasma interactions [1–5]. One of the most challenging applications driving recent activities is laser-based proton and/or ion acceleration for medical application in cancer therapy [6]. At currently available laser intensities, only indirect proton and/or ion acceleration is possible and it relies on the spatial and temporal dynamics of electrons that are directly accelerated by the laser pulse. The electric field induced by the charge separation between the remaining heavier ions and the fast moving electrons forms the driving force for accelerating protons. Two kinds of electrons, thermal and collective electrons [7], are responsible for the proton and/or ion acceleration. The ''thermal electrons'' are electrons having a high-temperature, broader energy distribution because of the collision and intensity-dependent heating, on the other hand the ''collective electrons'' are electrons having a low-temperature, narrow energy distribution pushed by the laser pulse as a whole. The electron properties depend on the laser and target parameters (e.g., peak intensity, contrast, polarization, spatial and temporal shape, target density, thickness, geometry, and atomic numbers of the constituents) [8,9].

Proton and/or ion acceleration by thermal electrons is known as target normal sheath acceleration (TNSA) [10–12] and is valid for solid targets with a wide thickness range: hundreds of nanometers to a few micrometers. In the TNSA scheme, the maximum proton energy is determined by the thermal electron temperature ($T_e = m_e c^2[(1 + a_0^2)^{1/2} - 1]$) [13], where m_e is the electron mass, c is the speed of light, and a_0 is the normalized laser amplitude. The proton energy should thus scale with the peak intensity in the form of $I^{1/2}$ [8]. Particle-in-cell (PIC) simulations have suggested that a maximum proton energy of >300 MeV should be possible at a peak intensity of 1×10^{22} W/cm^2, which is the highest laser intensity demonstrated [14]. Recently, a maximum proton energy of 40 MeV has been reported using micrometer-thick metal foils irradiated by 40-fs, 7.5-J laser pulses at 1×10^{21} W/cm^2 [15], but no energy scaling result was shown in that report.

Protons can be accelerated directly by a laser pulse at intensities of over 10^{24} W/cm^2. However, with a circularly polarized (CP) laser, the required intensity for proton/ion acceleration can be greatly reduced by the formation of an electrostatic field due to charge separation between ions and compressed electrons [16]. The use of a nanometer-scale ultrathin target with a CP laser pulse reduced the required intensity to the level of 10^{21} W/cm^2 [17]. This acceleration process is called the light-sail radiation pressure acceleration (LS-RPA) mechanism. According to the model, most electrons are collectively accelerated by the radiation pressure and the maximum proton energy linearly scales with the laser intensity I. The acceleration characteristics can be interpreted using the normalized areal density $\sigma = (n_e/n_c) \times (d/\lambda_L)$, where n_e is the electron density, n_c the critical density of plasma, d the target thickness, and λ_L the laser wavelength. Optimal conditions are obtained when the areal density (σ) is approximately equal to a_0. An RPA-like scheme has been demonstrated using a 5×10^{19} W/cm^2 CP laser pulse [18], in which a quasimonoenergetic C^{6+} ion spectrum and a significant reduction of thermal electrons were observed. However, due to the limited laser intensity, it was not possible to confirm the energy scaling and monoenergetic feature in the proton spectrum. Recent observation of

a narrow-band feature in the proton and/or ion energy spectrum was reported from an experiment using subpicosecond (700 fs), CP and linearly polarized (LP) laser pulses with a maximum intensity of 3×10^{20} W/cm^2 [19]. Alternative RPA schemes such as the hybrid RPA-TNSA [20,21] and leaky light-sail RPA [22] have been proposed for stable generation of high-energy monoenergetic proton and/or ion beams even at lower intensities (10^{20}–10^{21} W/cm^2) and/or with linear polarization.

In this Letter, we report on the experimental and simulation results for proton and/or ion acceleration from an ultrathin polymer target using 30-fs, LP, petawatt (PW) laser pulses. The aim of the experiments was to study, by measuring the proton energy scaling with respect to the laser intensity for different target thicknesses, the proton acceleration mechanism in the intensity range of 5×10^{19} W/cm^2 to 3.3×10^{20} W/cm^2 and to find out conditions for increasing the maximum proton energy with LP laser pulses. As a result of hybrid acceleration including TNSA, RPA, and Coulomb explosion assisted-free expansion, we were able to experimentally show, for the first time, the transition of proton energy scaling from $\sim I^{1/2}$ to $\sim I$ when a target with a thickness below 30 nm was irradiated by an ultraintense laser pulse. Two-dimensional (2D) and three-dimensional (3D) particle-in-cell (PIC) simulations were carried out under the same physical conditions to interpret the experimental results. Simulation results not only agreed well with the energy scaling regarding the laser intensity and target thickness, but also reproduced the structure of the proton spectra. Interesting features indicating RPA features such as linear energy scaling, quasimonoenergeticity, and a strong longitudinal electrostatic field by an electron-proton double layer is presented here, along with detailed numerical results and an interpretation.

Linearly polarized, 30-fs, 27-J laser pulses from the 1-PW, Ti:sapphire laser system (PULSER I) at the Advanced Photonics Research Institute were delivered to a double plasma mirror (DPM) system to enhance the temporal contrast ratio [23]. The overall output performances of the PW laser system are described elsewhere [24]. The DPM system had the same geometry as that used for the 100-TW laser system except for the size [25]. The contrast ratio measured after the DPM system was about 3×10^{-11} at 6 ps before the main pulse, which was enough for the application of ultrathin target such as 10 nm. After the DPM system, 30-fs, 8.3-J s-polarized laser pulses were focused onto ultrathin polymer targets (F8BT; see Ref. [23]) with thicknesses of 10, 20, 30, 50, 70, and 100 nm. The F8BT targets were fabricated from powder as McNeill *et al.* [26] did. They assumed the target density of F8BT as 1 g/cm^3. Based on this assumption, the calculated electron density (n_e) of F8BT was about $200n_c$. The surface topology of the target was described elsewhere [27,28]. The F8BT target was homogeneous in composition [hydrogen (55%) and carbon (45%)] because the chemical bonding between C and H was not broken during the fabrication process. The typical spot size in the focal plane was 5.8 μm (full width at half maximum), resulting in a maximum intensity of 3.3×10^{20} W/cm^2 ($a_0 = 12.4$). The laser pulses were incident on a target at an angle of 7° to the target normal to avoid retroreflection from the plasma on the target. During the experiment, the laser intensity was varied from 5×10^{19} ($a_0 = 4.8$) to 3.3×10^{20} W/cm^2 ($a_0 = 12.4$) without degrading the quality of focal spot by turning on pump-laser-beam lines sequentially. The proton and ion energy spectra were measured by a Thomson parabola equipped with a microchannel plate (MCP) and a charge-coupled device (CCD), and the absolute number calibration for the proton energy spectra was done by installing striped CR-39 track detectors in front of the MCP device [29].

The proton and carbon ion energy spectra obtained from a 10-nm-thick target irradiated at 3.3×10^{20} W/cm^2 are shown in Fig. 1(a). The maximum proton and C^{6+} ion energies were 45 and 164 MeV, respectively, which are the highest values ever reported from acceleration experiments using tens-of-femtosecond high-power laser pulses. For the 100-nm-thick target, maximum energies of 18 and 60 MeV were observed for the protons and C^{6+} ions, respectively. Figure 1(b) shows the maximum proton energies obtained at different target thicknesses and intensities. At a given intensity, the maximum proton energy generally increases as the target thickness decreases. In our case, the calculated optimum target thickness was 15.8 nm for F8BT when the relation $a_0 \sim \pi\sigma$ [30,31] was assumed at the intensity of 3.3×10^{20} W/cm^2 ($a_0 = 12.4$). However, since the optimum thickness was located in between 10 and 20 nm and the proton energy was sensitive to the target thickness in the vicinity of optimal thickness, we could not clarify the optimum thickness in the experiment.

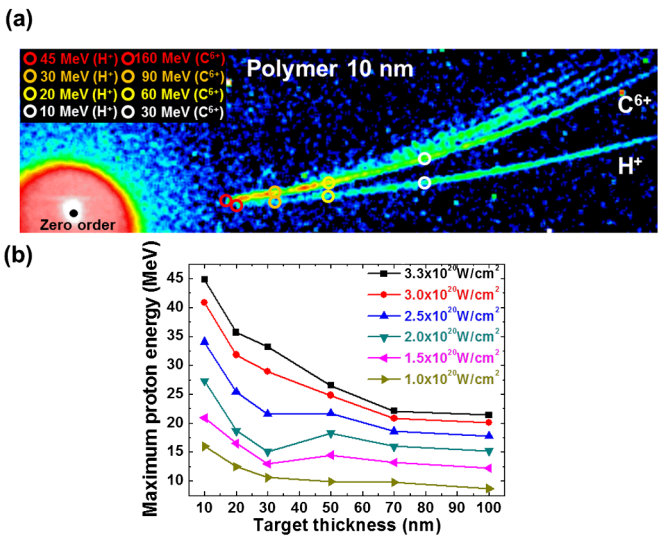

FIG. 1 (color online). Proton and C^{6+} energies measured from the Thomson parabola. (a) Energy spectra of the protons and carbon ions obtained from a 10-nm-thick target irradiated at 3.3×10^{20} W/cm^2. (b) Maximum proton energies obtained for different target thickness and intensities.

According to the previous results [18,32], a fine change (~3 nm) from an optimum target thickness (5.6 nm) resulted in the decrease of ~30% in the maximum proton energy. Thus, in our case, a fine interval (~5 nm when we consider the target density) of the target thickness might be required to investigate the maximum proton energy with an optimum target thickness. The other interesting feature in Fig. 1(b) is the proton energy dip observed with the 30-nm target under certain laser intensities. The same dip was also observed in the previous research [32]. However, 2D-PIC simulations could not very well explain the dip structure. More experiments and simulations are needed for understanding the physical origin of dip formation.

Figures 2(a) and 2(b) show the proton and C^{6+} ion energy spectra, respectively, obtained with the 10-nm- and 100-nm-thick targets irradiated at the highest intensity of 3.3×10^{20} W/cm^2. The proton spectrum of the 10-nm target showed a broad and modulated profile. PIC simulations have shown that a broad spectral profile results from the temporal evolution of electrons and protons during the acceleration process and that the modulation is related to the Rayleigh-Taylor (RT) instability (see details in the simulation part). Interestingly, for the 10-nm target, the quasimonoenergetic peaks (at 65, 91, and 120 MeV) in the C^{6+} ion spectrum are clearly visible in Fig. 2(b) and similar to those shown in Ref. [18]. This feature was observed in the successive measurements and may indicate evidence of the RPA mechanism under these conditions (a 10-nm- to 30-nm-thick target irradiated by a 3.3×10^{20} W/cm^2 LP laser pulse). For the 100-nm-thick target, however, the C^{6+} ion spectrum showed exponential decay, which is a typical feature of the TNSA mechanism. Despite the quasimonoenergetic feature in the ion spectrum, no obvious monoenergetic structure was observed in the proton energy spectrum even at the highest intensity (3.3×10^{20} W/cm^2). This phenomenon was also reproduced by 2D and 3D PIC simulations.

The dependence of the maximum proton energy on the laser intensity for the 10-, 20-, and 30-nm targets reveals the dominant acceleration mechanism in the proton acceleration stage which directly interacts with the laser field (see also [23] for the comparison). The maximum proton energy at each intensity shown in Fig. 3(a) is the average of three laser shots, and the error bars denote the standard deviations of the maximum proton energy and laser intensity. For these targets, the proton energy scaling shows a very important feature: at lower intensities, the maximum proton energy increased with intensity in the form $I^{1/2}$, and then linearly increased with intensity after a certain thickness-dependent-transition intensity. This behavior is explained by the transition of the dominant acceleration mechanism (from TNSA to RPA in the acceleration stage). The transition occurred at an intensity of approximately 1.75×10^{20} W/cm^2 for the 10-nm target, and the transition intensity increased by about 1.5×10^{19} W/cm^2 per 10 nm; thicker targets showed higher transition intensities due to the higher areal density. For the 20-nm and 30-nm targets, the energy scaling changes abruptly from $I^{1/2}$ to I, which implies that a small difference in the laser intensity may cause the significant change in the dominant acceleration. As shown in Fig. 3(b), the PIC simulations are in good agreement with the experimental results (see also [23] for the energy scaling of C^{6+} ions).

To interpret the experimental results, we carried out 2D- and 3D-PIC simulations (See also Ref. [23]) using ALPS code [33–35] showing the dynamics of the electrons, protons, and ions for both 10- and 30-nm targets irradiated by an ultraintense, ultrashort laser pulse. In the simulations, the peak intensity was varied from 5×10^{19} to 3.5×10^{20} W/cm^2 in a step of 5×10^{19} W/cm^2.

Figure 4 shows the 3D-PIC simulation results for the 10-nm-thick target irradiated at 3×10^{20} W/cm^2. The temporal evolutions of the electron and proton number densities for the 10-nm target are shown in Figs. 4(a) and 4(b). The acceleration dynamics can be described as follows: at 24 fs after the arrival of a laser pulse, a portion of electrons, heated by the oscillating component in the ponderomotive force, leave the target with a broad energy distribution (thermal electrons) in the forward and backward directions. At 36 fs, two different proton beam components appear in the interaction region: one due to the thermal electrons and the other due to the collective electrons. The thermal electrons drag protons in the forward and backward directions, and these protons obtain a broad momentum distribution (TNSA). The collective electrons pushed by radiation pressure contribute to form an electron-proton double layer [17,21] and drag protons to

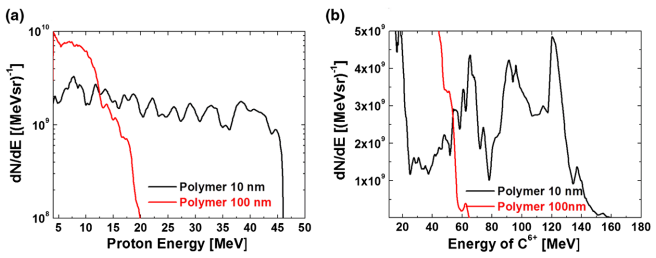

FIG. 2 (color online). Energy spectra of protons and C^{6+} ions obtained from 10- and 100-nm-thick targets. (a) Proton and (b) C^{6+} energy spectrum obtained with an intensity of 3.3×10^{20} W/cm^2.

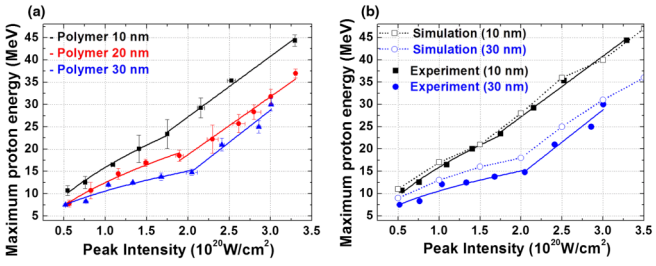

FIG. 3 (color online). Maximum proton energy as a function of the laser peak intensity for linearly polarized laser pulses. (a) Maximum proton energy for 10-, 20-, and 30-nm-thick polymer targets. (b) Comparison between the simulated and experimental results.

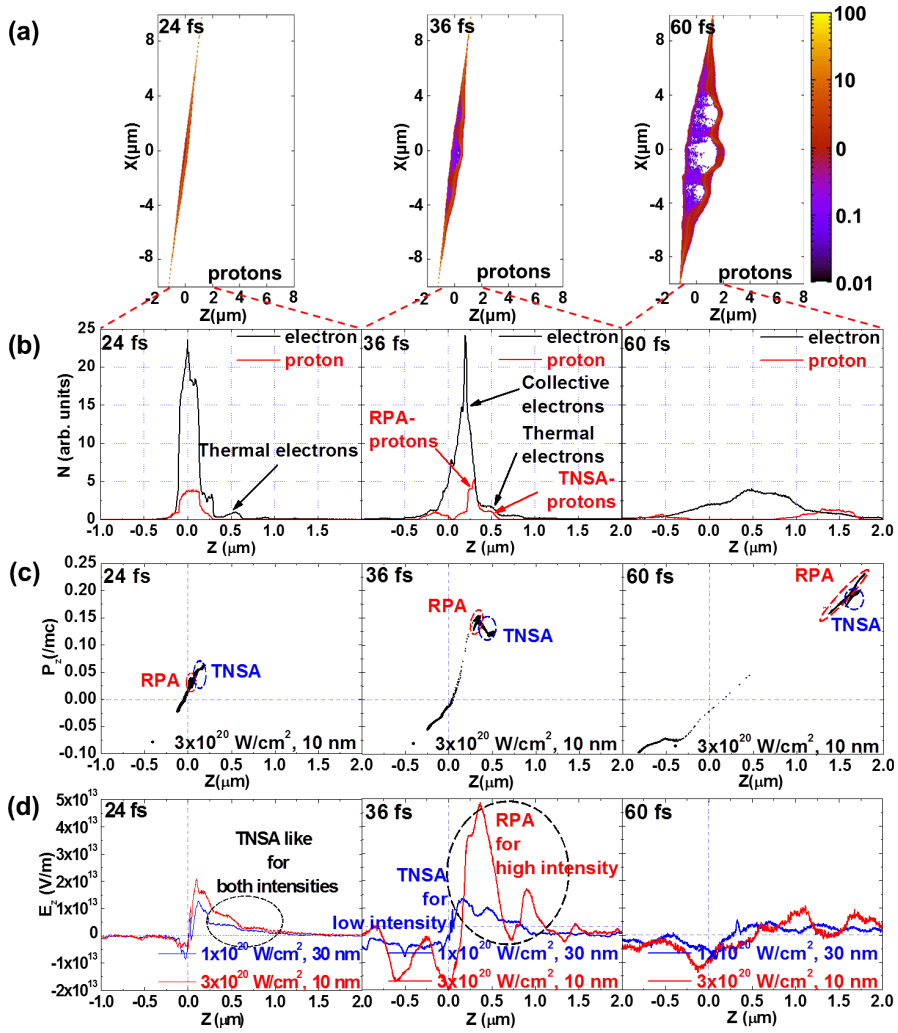

FIG. 4 (color online). PIC simulation results. Temporal evolutions of the number density of (a) protons and (b) its line profile over the central region with a 1-μm radius from a 10-nm target irradiated at 3.0×10^{20} W/cm^2. (c) The corresponding proton phase space distribution. (d) Temporal evolutions of the longitudinal electrostatic field for a 10-nm target irradiated at 3.0×10^{20} W/cm^2 and a 30-nm target irradiated at 1.0×10^{20} W/cm^2. Results are shown for $t = 24$, 36, and 60 fs after the interaction.

have a narrow momentum distribution (RPA) in the direction of the laser beam propagation. The thermal and collective electrons boost the proton energy up to 25 MeV until 60 fs, when the laser pulse ends at the surface of the target. The speed of protons accelerated by collective electrons overpasses the speed of protons by thermal electrons in this acceleration stage. The linear scaling of the proton energy with respect to the laser intensity is determined by the acceleration by collective electrons. At the same time the density modulation is initiated at a few tens of fs after the interaction. The origin of the modulation is the RT instability [36], and the modulation is responsible for the shape of proton energy spectrum mentioned above. However, the RT instability is not so critical to disturb the RPA process because the modulation by the RT instability is not so strong to break the proton layer during the RPA process. A rough estimation on the instability growth rate, $\Gamma \approx (ka)^{0.5}$, gives $\Gamma\tau_L \approx 1$, which means that the instability grows as $\sim e^1$ during the whole interaction and it is imprinted in the final proton distribution.

The proton acceleration continues as long as the laser intensity is high enough to maintain the double layer structure. At 60 fs, the collective electron layer smears out, and the proton acceleration by electrons is weakened due to the spatial broadening of the electrons. After the interaction ($t > 60$ fs), the protons are accelerated by the Coulomb explosion-assisted free expansion. In contrast, due to the high mass of carbon ions, the C^{6+} ions are not heavily influenced by thermal electrons, resulting in a quasimonoenergetic spectrum. According to the previous research [21], with a spatially trapezoidal laser pulse at a higher intensity of 10^{21} W/cm^2, the structure can be maintained for a longer time to produce GeV C^{6+} ions with quasimonoenergetic spectrum. For a 30-nm target irradiated by a 1×10^{20} W/cm^2 laser pulse, the collective electrons produced by the high-intensity part of the laser pulse are not sufficient and proton acceleration is dominated by the TNSA mechanism, as depicted in [23].

Figure 4(c) shows the temporal evolution of protons in the momentum space, for which the protons accelerated by collective electrons are faster than those accelerated by thermal electrons, leading to the linear energy scaling. The temporal evolutions of electric fields at two different conditions (30-nm target at 1×10^{20} W/cm^2 and 10-nm target at 3×10^{20} W/cm^2) are shown in Fig. 4(d). A strong longitudinal electrostatic field due to the electron-proton double layer is formed at an intensity of 3×10^{20} W/cm^2 and is maintained until the collective electrons are broadened. As shown in Figs. 4(c) and 4(d), thermal electrons

appear in the early stage of the interaction and contribute to the proton/ion acceleration during the whole process, while collective electrons appear in the high-intensity part and contribute to the proton and/or ion acceleration only in a specific time period. Consequently, it can be concluded that the collective electrons are responsible for the RPA features such as the linear scaling and quasimonoenergetic structure in the C^{6+} ion spectrum.

In conclusion, the experiments performed with LP 30-fs, 1-PW laser pulses have produced maximum proton and C^{6+} ion energies of 45 and 164 MeV, respectively, at a laser intensity of 3.3×10^{20} W/cm^2. The change in the energy scaling obtained from a target with a thickness below 30 nm indicated a transition of the dominant acceleration mechanism (i.e., from TNSA to RPA) and a further acceleration by Coulomb explosion-assisted free expansion (in the postacceleration stage) was responsible for the maximum proton energy. The 2D- and 3D-PIC simulations gave a detailed understanding of the acceleration dynamics, and reproduced the spectra and the energy scaling that agreed well with the experimental results. Assuming the validity of the measured linear scaling for the ultrathin polymer target, a proton energy of 190 MeV and a C^{6+} ion energy of 730 MeV should be possible at an intensity of 1.5×10^{21} W/cm^2, which is expected to be available soon [37]. Such a high value of particle energy will create a breakthrough for cancer treatments using laser-accelerated protons and/or ions, and thus further experimental studies on linear scaling at higher laser intensity are of crucial importance.

We thank Prof. C. H. Nam for the fruitful discussions. This work was supported by the Ministry of Knowledge and Economy of Korea through the Ultrashort Quantum Beam Facility Program. And this work was supported by Institute for Basic Science (IBS-CA1306). This work was also supported by Applications of Femto-Science to Nano/bio-Technology Utilizing Ultrashort Quantum Beam Facility through a grant provided by GIST. P. V. N. acknowledges support of the World Class University program (R31-2008-000-10026-0) grant provided by National Research Foundation (NRF) of Korea.

*jeongtm@gist.ac.kr
†leejm@gist.ac.kr

[1] S. P. D. Mangles *et al.*, Nature (London) **431**, 535 (2004).
[2] C. G. R. Geddes, Cs. Toth, J. van Tilborg, E. Esarey, C. B. Schroeder, D. Bruhwiler, C. Nieter, J. Cary, and W. P. Leemans, Nature (London) **431**, 538 (2004).
[3] J. Faure, Y. Glinec, A. Pukhov, S. Kiselev, S. Gordienko, E. Lefebvre, J.-P. Rousseau, F. Burgy, and V. Malka, Nature (London) **431**, 541 (2004).
[4] B. M. Hegelich, B. J. Albright, J. Cobble, K. Flippo, S. Letzring, M. Paffett, H. Ruhl, J. Schreiber, R. K. Schulze, and J. C. Fernández, Nature (London) **439**, 441 (2006).
[5] H. Schwoerer, S. Pfotenhauer, O. Jäckel, K.-U. Amthor, B. Liesfeld, W. Ziegler, R. Sauerbrey, K. W. D. Ledingham, and T. Esirkepov, Nature (London) **439**, 445 (2006).
[6] S. V. Bulanov and V. S. Khoroshkov, Plasma Phys. Rep. **28**, 453 (2002).
[7] T. Tajima, D. Habs, and X. Yan, Rev. Accel. Sci. Tech. **02**, 201 (2009).
[8] J. Fuchs *et al.*, Nat. Phys. **2**, 48 (2006).
[9] L. Robson *et al.*, Nat. Phys. **3**, 58 (2007).
[10] S. P. Hatchett *et al.*, Phys. Plasmas **7**, 2076 (2000).
[11] S. C. Wilks, A. B. Langdon, T. E. Cowan, M. Roth, M. Singh, S. Hatchett, M. H. Key, D. Pennington, A. MacKinnon, and R. A. Snavely, Phys. Plasmas **8**, 542 (2001).
[12] M. Passoni, L. Bertagna, and A. Zani, New J. Phys. **12**, 045012 (2010).
[13] S. C. Wilks, W. L. Kruer, M. Tabak, and A. B. Langdon, Phys. Rev. Lett. **69**, 1383 (1992).
[14] S.-W. Bahk, P. Rousseau, T. A. Planchon, V. Chvykov, G. Kalintchenko, A. Maksimchuk, G. A. Mourou, and V. Yanovsky, Opt. Lett. **29**, 2837 (2004).
[15] K. Ogura *et al.*, Opt. Lett. **37**, 2868 (2012).
[16] A. Macchi, F. Cattani, T. V. Liseykina, and F. Cornolti, Phys. Rev. Lett. **94**, 165003 (2005).
[17] A. P. L. Robinson, M. Zepf, S. Kar, R. G. Evans, and C. Bellei, New J. Phys. **10**, 013021 (2008).
[18] A. Henig *et al.*, Phys. Rev. Lett. **103**, 245003 (2009).
[19] S. Kar *et al.*, Phys. Rev. Lett. **109**, 185006 (2012).
[20] H. B. Zhuo, Z. L. Chen, W. Yu, Z. M. Sheng, M. Y. Yu, Z. Jin, and R. Kodama, Phys. Rev. Lett. **105**, 065003 (2010).
[21] B. Qiao, S. Kar, M. Geissler, P. Gibbon, M. Zepf, and M. Borghesi, Phys. Rev. Lett. **108**, 115002 (2012).
[22] B. Qiao, M. Zepf, M. Borghesi, B. Dromey, M. Geissler, A. Karmakar, and P. Gibbon, Phys. Rev. Lett. **105**, 155002 (2010).
[23] See Supplemental Material at http://link.aps.org/supplemental/10.1103/PhysRevLett.111.165003 for the explanation on the laser system, diagnostics, target, and simulation parameters in detail.
[24] J. H. Sung, S. K. Lee, T. J. Yu, T. M. Jeong, and J. Lee, Opt. Lett. **35**, 3021 (2010).
[25] I. J. Kim, I. W. Choi, S. K. Lee, K. A. Janulewicz, J. H. Sung, T. J. Yu, H. T. Kim, H. Yun, T. M. Jeong, and J. Lee, Appl. Phys. B **104**, 81 (2011).
[26] C. R. McNeill, B. Watts, L. Thomsen, H. Ade, N. C. Greenham, and P. C. Dastoor, Macromolecules **40**, 3263 (2007).
[27] I. W. Choi *et al.*, Appl. Phys. Lett. **99**, 181501 (2011).
[28] C.-L. Lee, X. Yang, and N. C. Greenham, Phys. Rev. B **76**, 245201 (2007).
[29] R. Prasad *et al.*, Nucl. Instrum. Methods Phys. Res., Sect. A **623**, 712 (2010).
[30] A. Macchi, S. Veghini, and F. Pegoraro, Phys. Rev. Lett. **103**, 085003 (2009).
[31] H. Daido, M. Nishiuchi, and A. S Pirozhkov, Rep. Prog. Phys. **75**, 056401 (2012).
[32] S. Steinke *et al.*, Laser Part. Beams **28**, 215 (2010).
[33] K. H. Pae, I. W. Choi, and J. Lee, Phys. Plasmas **17**, 123104 (2010).
[34] K. H. Pae, I. W. Choi, and J. Lee, Laser Part. Beams **29**, 11 (2011).
[35] I. J. Kim *et al.*, Nat. Commun. **3**, 1231 (2012).
[36] F. Pegoraro and S. V. Bulanov, Phys. Rev. Lett. **99**, 065002 (2007).
[37] T. J. Yu, S. K. Lee, J. H. Sung, J. W. Yoon, T. M. Jeong, and J. Lee, Opt. Express **20**, 10 807 (2012).